

Lattice thermal conductivity of β_{12} and χ_3 borophene

Jia He(何佳), Yulou Ouyang(欧阳宇楼), Cuiqian Yu(俞崔前), Pengfei Jiang(蒋鹏飞), Weijun Ren(任卫君), and Jie Chen(陈杰)†

Citation: Chin. Phys. B, 2020, 29 (**12**): 126503. DOI: 10.1088/1674-1056/abbbe6
Journal homepage: http://cpb.iphy.ac.cn; http://iopscience.iop.org/cpb

What follows is a list of articles you may be interested in

Lattice thermal conductivity of β_{12} and χ_3 borophene

Jia He(何佳), Yulou Ouyang(欧阳宇楼), Cuiqian Yu(俞崔前), Pengfei Jiang(蒋鹏飞), Weijun Ren(任卫君), and Jie Chen(陈杰)†
Chin. Phys. B, 2020, 29 (**12**): 126503. DOI: 10.1088/1674-1056/abbbe6

Tuning thermal transport via phonon localization in nanostructures

Dengke Ma(马登科), Xiuling Li(李秀玲)†, and Lifa Zhang(张力发)\cclink
Chin. Phys. B, 2020, 29 (**12**): 126502. DOI: 10.1088/1674-1056/abb7fa

Low lattice thermal conductivity and high figure of merit in p-type doped K_3IO

Weiqiang Wang(王巍强), Zhenhong Dai(戴振宏), Qi Zhong(钟琦), Yinchang Zhao(赵银昌), and Sheng Meng(孟胜)
Chin. Phys. B, 2020, 29 (**12**): 126501. DOI: 10.1088/1674-1056/abab

Ultra-low thermal conductivity of roughened silicon nanowires: Role of phonon-surface bond order imperfection scattering

Heng-Yu Yang(杨恒玉), Ya-Li Chen(陈亚利), Wu-Xing Zhou(周五星), Guo-Feng Xie(谢国锋), Ning Xu(徐宁)
Chin. Phys. B, 2020, 29 (**8**): 086502. DOI: 10.1088/1674-1056/ab99af

Effects of surface charges on phonon properties and thermal conductivity in GaN nanofilms

Shu-Sen Yang(杨树森), Yang Hou(侯阳), Lin-Li Zhu(朱林利)
Chin. Phys. B, 2019, 28 (**8**): 086501. DOI: 10.1088/1674-1056/28/8/086501

SPECIAL TOPIC — Phononics and phonon engineering

Lattice thermal conductivity of β_{12} and χ_3 borophene*

Jia He(何佳), Yulou Ouyang(欧阳宇楼), Cuiqian Yu(俞崔前), Pengfei Jiang(蒋鹏飞), Weijun Ren(任卫君), and Jie Chen(陈杰)†

Center for Phononics and Thermal Energy Science, China–EU Joint Laboratory for Nanophononics, School of Physics Science and Engineering, Tongji University, Shanghai 200092, China

(Received 26 June 2020; revised manuscript received 13 September 2020; accepted manuscript online 28 September 2020)

Borophene allotropes have many unique physical properties due to their polymorphism and similarity between boron and carbon. In this work, based on the density functional theory and phonon Boltzmann transport equation, we investigate the lattice thermal conductivity κ of both β_{12} and χ_3 borophene. Interestingly, these two allotropes with similar lattice structures have completely different thermal transport properties. β_{12} borophene has almost isotropic κ around 90 W/(m·K) at 300 K, while κ of χ_3 borophene is much larger and highly anisotropic. The room temperature κ of χ_3 borophene along the armchair direction is 512 W/(m·K), which is comparable to that of hexagonal boron nitride but much higher than most of the two-dimensional materials. The physical mechanisms responsible for such distinct thermal transport behavior are discussed based on the spectral phonon analysis. More interestingly, we uncover a unique one-dimensional transport feature of transverse acoustic phonon in χ_3 borophene along the armchair direction, which results in a boost of phonon relaxation time and thus leads to the significant anisotropy and ultrahigh thermal conductivity in χ_3 borophene. Our study suggests that χ_3 borophene may have promising application in heat dissipation, and also provides novel insights for enhancing the thermal transport in two-dimensional systems.

Keywords: borophene, thermal conductivity, two-dimensional (2D) material, density functional theory

PACS: 65.80.–g **DOI:** 10.1088/1674-1056/abbbe6

1. Introduction

Due to the device miniaturization and escalated power density, the nanoscale thermal management[1–4] has been crucial in the development of nanoelectronic devices. Carbon-based materials have high thermal conductivity due to their strong covalent bonds, such as diamond[5,6] ∼ 2000 W/(m·K), carbon nanotubes[7,8] ∼ 3000 W/(m·K), and graphene[9–14] ∼3000–5000 W/(m·K). The unique thermal and electrical properties of graphene have opened the age of two-dimensional materials,[15–25] such as transition metal dichalcogenides,[26] black phosphorene,[27,28] and hexagonal boron nitride (h-BN).[29,30] As the neighbor of the carbon in the periodic table, monolayer of boron, namely, borophene, may also have high thermal conductivity due to its light atomic mass and short covalent bond.

Recently, three types of borophene allotropes (namely, δ_6, β_{12}, and χ_3) have been grown on Ag (111) substrate,[31,32] as a result of the multicenter bond of boron.[33] Freestanding β_{12} and χ_3 borophene can also be synthesized by a novel liquid-phase exfoliation.[34] Theoretical calculations indicate the strong electron–phonon coupling in borophene,[35,36] which may lead to a significant decrease of the thermal conductivity.[37,38] More interestingly, the existence of gapless Dirac cones has been reported,[39–41] which were observed experimentally by the angle-resolved photoemission spectroscopy in β_{12} and χ_3 borophene.[42,43] These results suggest that borophene can be used in the new-generation high-speed low-dissipation electronic devices. Besides, borophene has also been used in hydrogen storage,[44] rechargeable metal-ion batteries,[45] and mechanically robust components.[46]

In terms of phononic thermal transport, thermal conductivity of borophene may vary greatly in different structures and directions due to its high anisotropy and polymorphic structures. With non-equilibrium Green's function approach, the ballistic thermal conductances of δ_6 and β_{12} borophene have been calculated at low temperature, which are found to be higher than that of graphene.[47–49] However, the thermal conductivity of δ_6 borophene when considering the lattice anharmonicity is much lower than that of graphene.[50] The structure of δ_6 borophene does not have mirror symmetry, resulting in a strong scattering for ZA phonons and thus a lower thermal conductivity.[51] The other two types of synthesized borophene allotropes (β_{12} and χ_3) have planar structures that can satisfy the mirror symmetry condition. However, their diffusive thermal transport properties are still unknown, which are of particular importance for practical applications as the

*Project supported in part by the National Key Research and Development Program of China (Grant No. 2016YFA0200901), the National Natural Science Foundation of China (Grant No. 11890703), the Science and Technology Commission of Shanghai Municipality, China (Grant Nos. 19ZR1478600 and 18JC1410900), the Fundamental Research Funds for the Central Universities, China (Grant No. 22120200069), and the Open Fund of Hunan Provincial Key Laboratory of Advanced Materials for New Energy Storage and Conversion (Grant No. 2018TP1037_201901).

†Corresponding author. E-mail: jie@tongji.edu.cn

© 2020 Chinese Physical Society and IOP Publishing Ltd

anharmonic phonon–phonon interaction might not be negligible at finite temperature.

In this work, the lattice thermal conductivities of β_{12} and χ_3 borophene are studied by using density functional theory and phonon Boltzmann transport equation. Our calculation results indicate that thermal transport behaviors in these two borophene allotropes are quite different, although their lattice structures look similar. The thermal transport in χ_3 borophene is highly anisotropic, with its room temperature thermal conductivity in the armchair direction comparable to that of h-BN ~ 600 W/(m·K). However, the thermal conductivity of β_{12} borophene is almost isotropic and much lower than that of χ_3 borophene. The physical mechanisms responsible for the different anisotropic transport behaviors and thermal conductivities are revealed by analyzing the phonon properties. Interestingly, we uncover a unique one-dimensional heat conduction mechanism in χ_3 borophene, which may provide important insights to the enhancement of thermal transport in two-dimensional systems.

2. Computational method

All first-principles calculations are performed based on density functional theory (DFT) as implemented in the Quantum ESPRESSO.[52] Ultrasoft pseudopotentials are used for all atoms, and the exchange–correlation approximation is described by the Perdew–Burke–Ernzerh (PBE) functional. The cutoff energy of plane-waves is set to be 50 Ry. The convergence criteria for energies and forces are set to be 10^{-6} Ry and 10^{-5} Ry per Bohr, respectively. A vacuum layer with the thickness of 20 Å is adopted in the direction perpendicular to the borophene sheet.

The lattice thermal conductivity of borophene is calculated by using the ShengBTE code,[53,54] which implements a fully iterative solution of the Boltzmann transport equation (BTE). The second order interatomic force constants are computed from the first-principles calculations based on the density functional perturbation theory (DFPT). A q-mesh grid of $5\times5\times1$ is used for β_{12} borophene, while a q-mesh grid of $5\times5\times1$ is used for χ_3 borophene. The third-order anharmonic force constants are calculated via finite displacement method by combining third-order and DFT in Quantum ESPRESSO, $5\times7\times1$ ($3\times9\times1$) supercells and $5\times5\times1$ ($5\times5\times1$) k-meshes are used to ensure the convergence of calculation for β_{12} (χ_3) borophene. We include the interactions within the 10th nearest-neighbour atoms, and choose a $61\times61\times1$ q-mesh for phonon–phonon scattering calculation. When calculating the volume of borophene, the thickness of borophene is defined as the van der Waals diameter for a boron atom[55] of 3.6 Å. Recent studies have found that four-phonon scattering can have significant impact on the thermal conductivity of bulk boron arsenide and silicon at high temperature.[56–60] However, we limit our discussion based on the three-phonon scattering process in this work, due to the computational complexity and high cost for handling higher-order anharmonic phonon–phonon interaction, which might be worth investigating in future study.

Based on the BTE, the lattice thermal conductivity tensor ($\kappa_{\alpha\beta}$) can be described as[53,54]

$$\kappa_{\alpha\beta}=\frac{1}{k_{\mathrm{B}}T^2NV}\sum_{\lambda}f_0(f_0+1)(\hbar\omega_\lambda)^2v_\lambda^\alpha F_\lambda^\beta, \tag{1}$$

where f, k_{B}, T, V, $\hbar$, and N are the phonon distribution function, the Boltzmann constant, temperature, the volume of the unit cell, the reduced Plank constant, and the total number of q-points, respectively. Here, ω_λ denotes the frequency of a phonon mode λ that is uniquely defined by the phonon branch s and wave vector q in the Brillouin zone, υ_λ^α is the phonon group velocity in the α-direction, and F_λ^β is given by

$$F_\lambda^\beta=\tau_\lambda^0\left(v_\lambda^\beta+\Delta_\lambda^\beta\right), \tag{2}$$

where τ_λ^0 is the phonon lifetime which is obtained by the relaxation time approximation, and Δ_λ^β is a correction term obtained by the fully iterative solution of BTE.[53]

The anharmonic three-phonon scattering process is the dominating scattering mechanism in pristine crystals, and the resulting phonon lifetime can be calculated based on the Fermi golden rule[54,61] as

$$\tau_\lambda^{\mathrm{ph}}=N\left(\sum_{\lambda_1\lambda_2}\Gamma^+_{\lambda\lambda_1\lambda_2}+\frac{1}{2}\sum_{\lambda_1\lambda_2}\Gamma^-_{\lambda\lambda_1\lambda_2}\right)^{-1}, \tag{3}$$

where $\Gamma^+_{\lambda\lambda_1\lambda_2}$ and $\Gamma^-_{\lambda\lambda_1\lambda_2}$ represent the scattering rates for the absorbing and emitting three-phonon scattering processes, respectively. The phonon scattering rates are given by

$$\begin{aligned}\Gamma^+_{\lambda\lambda_1\lambda_2}&=\frac{\hbar\pi}{4}\frac{\left(f_0^{\lambda_1}-f_0^{\lambda_2}\right)}{\omega_\lambda\omega_{\lambda_1}\omega_{\lambda_2}}\left|V^+_{\lambda\lambda_1\lambda_2}\right|^2\\&\quad\times\delta(\omega_\lambda+\omega_{\lambda_1}-\omega_{\lambda_2}),\end{aligned} \tag{4}$$

$$\begin{aligned}\Gamma^-_{\lambda\lambda_1\lambda_2}&=\frac{\hbar\pi}{4}\frac{\left(f_0^{\lambda_1}+f_0^{\lambda_2}+1\right)}{\omega_\lambda\omega_{\lambda_1}\omega_{\lambda_2}}\left|V^-_{\lambda\lambda_1\lambda_2}\right|^2\\&\quad\times\delta\left(\omega_\lambda-\omega_{\lambda_1}-\omega_{\lambda_2}\right).\end{aligned} \tag{5}$$

The $V^\pm_{\lambda\lambda_1\lambda_2}$ is the scattering matrix element and given by[62]

$$V^\pm_{\lambda\lambda_1\lambda_2}=\sum_{i,j,k}\sum_{\alpha\beta\gamma}\Phi^{\alpha\beta\gamma}_{ijk}\frac{e^{i\alpha}_\lambda e^{j\beta}_{\pm\lambda_1}e^{k\gamma}_{-\lambda_2}}{\sqrt{m_im_jm_k}}, \tag{6}$$

where i, j, and k are the atomic indices; m is the atomic mass; and $e^{i\alpha}_\lambda$ is the α-th component of the phonon eigenvector on the atom.

3. Results and discussion

Figures 1(a) and 1(b) show the lattice structures of β_{12} and χ_3 borophene, respectively. Both of them have a purely planar surface. The structures of β_{12} and χ_3 are very similar, except for the concentration of hexagonal holes. The optimized lattice constants in our calculations are shown in Table 1, which are in excellent agreement with the literature results.[32,35,63] Moreover, the calculated phonon dispersion (see Fig. 2) reveals that in addition to the two acoustic branches with linear dispersion for the in-plane modes (longitudinal acoustic and transverse acoustic modes, LA and TA), both allotropes have the third out-of-plane branch (flexural acoustic mode, ZA) with a quadratic dispersion, which is a typical signature of two-dimensional (2D) materials.[64] The cut-off frequency in the phonon dispersion is 34 THz and 38 THz for β_{12} and χ_3 borophene, respectively, which is lower than that in graphene[48] around 48 THz.

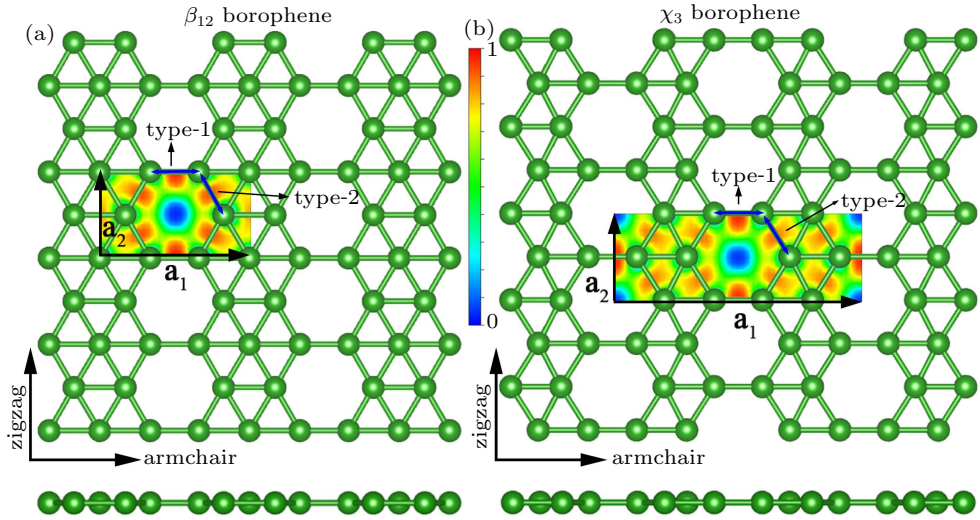


Fig. 1. Top and side views of lattice structures for (a) β_{12} and (b) χ_3 borophene. The side views show that both β_{12} and χ_3 borophene have purely planar structures. The contours illustrate the electron localization function (ELF) distribution.

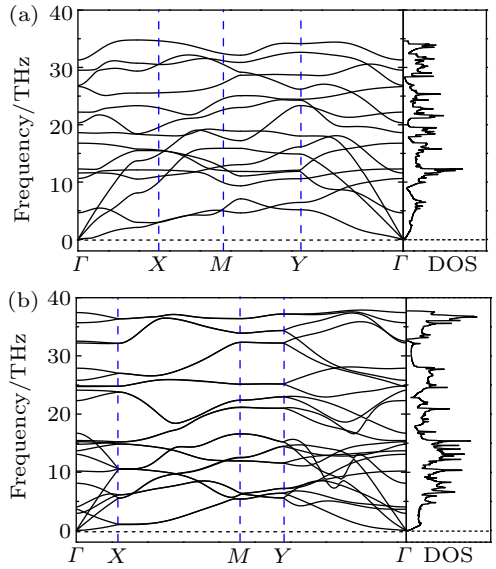


Fig. 2. Phonon dispersion and density of states of (a) β_{12} and (b) χ_3 borophene.

Table 1. The lattice constants for β_{12} and χ_3 borophene.

	a_1/Å	a_2/Å	Source
β_{12} borophene	5.06	2.92	this work
	5.07	2.93	Refs. [32,35]
χ_3 borophene	8.42	2.90	this work
	8.43	2.90	Refs. [32,63]

We then calculate the thermal conductivity along the armchair and zigzag directions for both β_{12} and χ_3 borophene by using the iterative solution to BTE. As shown in Fig. 3, at high temperatures, the thermal conductivities of both borophene allotropes follow the $\kappa \sim T^{-1}$ law quite well, indicating the dominance of three-phonon scattering at high temperature. The thermal conductivity of β_{12} borophene is almost isotropic, which has the room temperature thermal conductivity of 88 W/(m·K) and 94 W/(m·K) along the armchair and zigzag directions (solid line in Fig. 3(a)), respectively. In sharp contrast, thermal transport in χ_3 borophene is highly anisotropic, with thermal conductivity along the armchair direction notably higher than that along the zigzag direction. At room temperature, thermal conductivity of χ_3 borophene is 512 W/(m·K) and 312 W/(m·K) for the armchair and zigzag directions (solid line in Fig. 3(b)), respectively. However, the lattice structures of β_{12} and χ_3 borophene are very similar. In addition, their mechanical properties are also similar, including Young's modulus, Poisson's ratio, bending stiffness, and mass density.[65] Therefore, it is quite unexpected that β_{12} and χ_3 borophene have such distinct thermal transport properties.

Compared to other 2D materials, such as graphene[51,66] $\sim$ 3000 W/(m·K), hexagonal boron nitride[67] $\sim$ 600 W/(m·K), hydrogen boride[68] $\sim$ 334 W/(m·K) for the zigzag direction, borophane[69] $\sim$ 265 W/(m·K) for the zigzag direction, monolayer molybdenum disulfide[70] $\sim$ 87 W/(m·K),

phosphorene[71] ∼ 30 W/(m·K) for the zigzag direction, and stanene[72] ∼12 W/(m·K), we find that thermal conductivity of χ_3 borophene is about one-sixth that of graphene, comparable to that of hexagonal boron nitride, but is far higher than that of the rest 2D materials. It is worth to point out that the thermal conductivity of χ_3 borophene along the armchair direction is the highest among all 2D boron-materials reported so far.[33]

Table 2. Acoustic phonon group velocities near the Γ point in β_{12} and χ_3 borophene.

	ZA/(km/s)	LA/(km/s)	TA/(km/s)
β_{12}-armchair	6.5	13.1	16.8
β_{12}-zigzag	7.2	11.1	17.6
χ_3-armchair	2.4	11.8	18.0
χ_3-zigzag	4.1	11.4	17.7

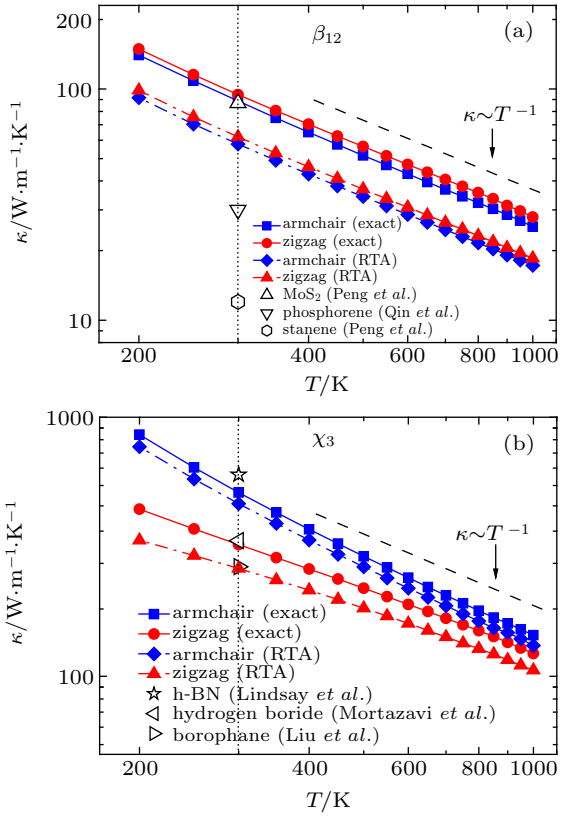


Fig. 3. The temperature dependence of lattice thermal conductivity in (a) β_{12} and (b) χ_3 borophene. The solid line and dash-dot line denote the calculation results of iterative solution and relaxation time approximation, respectively. The dashed lines indicate the $\kappa \sim T^{-1}$ dependence. The empty symbols show the room temperature thermal conductivity of other 2D materials recorded in literatures[67–72] for comparison.

To understand the dissimilarity of thermal conductivity and the anisotropy behavior, we first look into the harmonic phonon property, i.e., phonon group velocity. No substantially difference is observed in the phonon group velocity between β_{12} and χ_3 borophene (see Fig. 4). For instance, the group velocities for TA phonons in the long-wavelength limit along the armchair direction are 16.8 km/s and 18 km/s for β_{12} borophene and χ_3 borophene (Table 2), with only 7% difference. Similar result is obtained for other phonon branches. Given the obvious difference in thermal conductivity between two allotropes (Fig. 3), we conclude that the phonon group velocity is not the major cause responsible for the observed dissimilar thermal transport behavior.

Moreover, we notice that the anisotropic ratio of thermal conductivity in χ_3 borophene gradually decreases with the increase of temperature, as shown in Fig. 3(b). This is because the contribution of high-frequency phonons to the thermal conductivity becomes more significant at elevated temperature. For high-frequency phonons (above 30 THz) in χ_3 borophene, the phonon group velocity in zigzag direction is notably larger than that in armchair direction (Fig. 4(b)). As a result, although thermal conductivity in both directions decreases with increasing temperature due to the enhanced phonon–phonon scattering, thermal conductivity in zigzag direction decreases slower than that in armchair direction, due to the contribution of high-frequency phonons at high temperature, leading to the reduced anisotropic ratio in χ_3 borophene with increasing temperature.

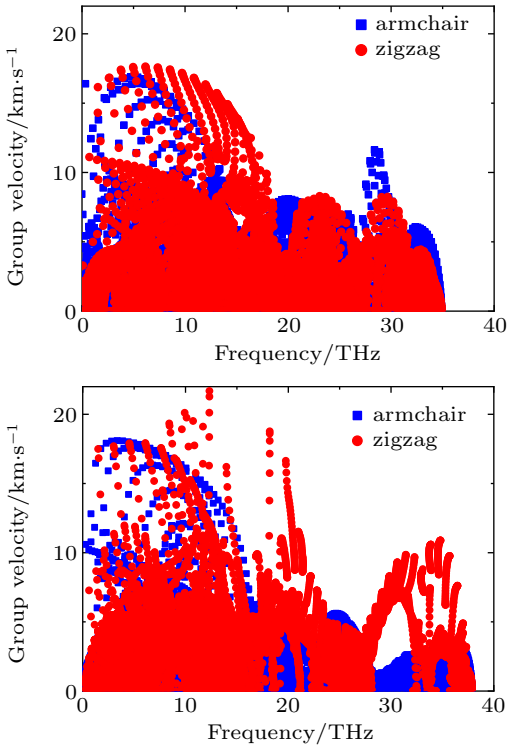


Fig. 4. The group velocities of (a) β_{12} and (b) χ_3 borophene.

To understand the impact of anharmonic phonon–phonon interactions, we then investigate the relaxation time in both borophene allotropes. For β_{12} borophene (Fig. 5(a)), the relaxation time of ZA phonon is as high as 1000 ps, which is about 2 orders of magnitude greater than that of other phonon branches. This result implies that the ZA phonon may make the dominant contribution to the thermal conductivity of β_{12} borophene. For χ_3 borophene (Fig. 5(b)), the maximum relaxation time of ZA phonon is even one order of magnitude

greater than that in β_{12} borophene, and reaches up to 14000 ps. Meanwhile, the relaxation time of LA and TA phonons in χ_3 borophene is also notably larger than that in β_{12} borophene. One peculiar feature observed for χ_3 borophene is the remarkably large relaxation time up to 6000 ps for some of the low-frequency TA phonons (dashed ellipse in Fig. 5(b)), which suggests that the TA phonon may have significant contribution to thermal conductivity of χ_3 borophene.

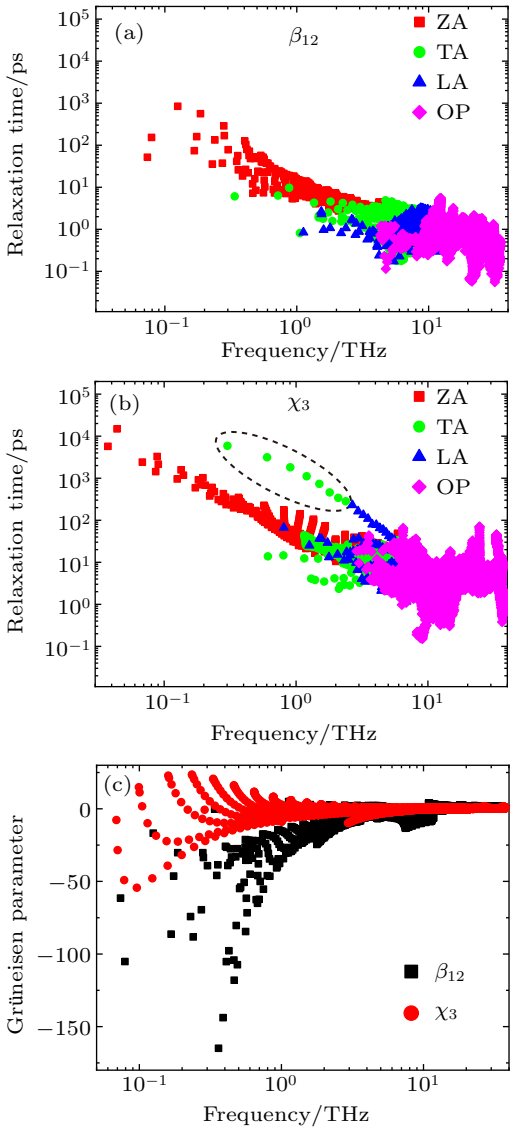


Fig. 5. The phonon relaxation time in (a) β_{12} and (b) χ_3 borophene at 300 K. The dashed ellipse in (b) highlights the low-frequency TA phonon with very long relaxation time. (c) The Grüneisen parameters of β_{12} and χ_3 borophene at 300 K.

In order to deeply elucidate the different phonon relaxation time, we plot in Fig. 5(c) the Grüneisen parameter which quantifies the degree of anharmonicity. The largest Grüneisen parameter in χ_3 borophene is only about 30% of that in β_{12} borophene. Obviously, the Grüneisen parameters for low frequency phonons in β_{12} borophene are substantially larger compared to those in χ_3 borophene, suggesting a stronger anharmonic phonon–phonon interaction in β_{12} borophene. The lager phonon anharmonicity causes stronger phonon–phonon scattering and leads to the smaller relaxation time observed in β_{12} borophene, which is responsible for the lower thermal conductivity of β_{12} borophene compared to that of χ_3 borophene.

Next, we investigate the contribution of different phonons by looking at the cumulative thermal conductivity with respect to phonon frequency. As shown in Fig. 6(a), the thermal conductivity of β_{12} borophene is mostly contributed ($\sim 88\%$) by phonons with frequency lower than 10 THz, which is close to the upper limit of this acoustic phonon branch. Therefore, acoustic phonons make the dominant contribution to the thermal conductivity of β_{12} borophene. However, the situation in χ_3 borophene is quite different. As shown in Fig. 6(b), the cumulative thermal conductivity saturates when the phonon frequency is larger than 15 THz, while the cutoff frequency for the acoustic phonon is only 6.1 THz. This means that the optical phonons make notable contribution to the thermal conductivity of χ_3 borophene, particularly in the zigzag direction. More interestingly, we notice that in the armchair direction which has a high thermal conductivity of 512 W/(m·K) at 300 K, the low-frequency acoustic phonons in the range of 0.3 THz–2.3 THz (dashed box in Fig. 6(b)) surprisingly contribute about 50% thermal conductivity of χ_3 borophene in the armchair direction. We have verified that these low-frequency phonons actually correspond to the low-frequency TA phonons with very large relaxation time (dashed ellipse in Fig. 5(b)). This result suggests that the TA phonons play a significant role in the thermal transport along the armchair direction of χ_3 borophene.

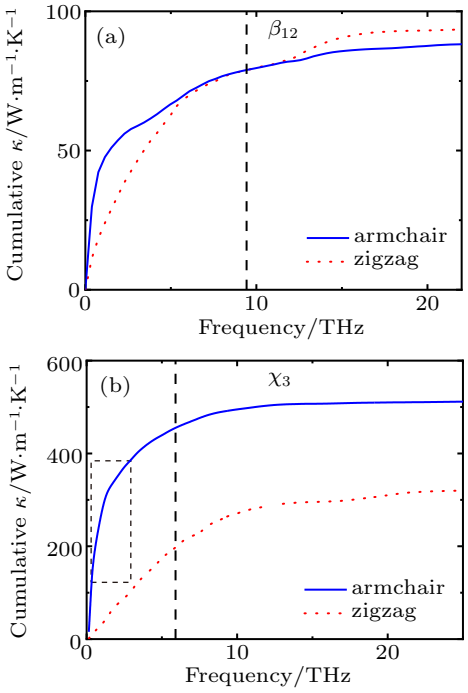


Fig. 6. The room temperature cumulative lattice thermal conductivity as a function of phonon frequency for (a) β_{12} and (b) χ_3 borophene. The vertical dashed line indicates the cutoff frequency of acoustic branches. The dashed box in (b) highlights the area of interest for comparison.

The isotropic thermal conductivity in β_{12} borophene and anisotropic thermal conductivity in χ_3 borophene can be understood by analyzing the lattice structure. To explore the underlying mechanism from the perspective of bonding electrons of neighboring atoms, we calculate the distribution of electron localization function (ELF) which takes a value between 0 and 1, with ELF = 1 denoting perfect localization, and ELF = 0 denoting no electron.[73] For β_{12} borophene, the bond lengths for two types of B–B bonds in different directions are very close to each other (1.66 Å for type-1 and 1.69 Å for type-2). Moreover, the ELF distribution along different directions is also similar (Fig. 1(a)), which indicates the isotropic thermal transport in β_{12} borophene. In contrast, the B–B bond lengths in different directions of χ_3 borophene are notably different (1.62 Å for type-1 and 1.72 Å for type-2), and the ELF distribution shown in Fig. 1(b) reveals that the electron localization of type-1 bond along armchair direction is stronger than that of type-2 bond along zigzag direction, indicating the anisotropic thermal transport in χ_3 borophene.

To further identify the source for the difference in the anisotropic thermal transport, we decompose the total thermal conductivity into branch contributions for both borophene allotropes. For β_{12} borophene (Fig. 7(a)), ZA phonon makes the dominant contribution to thermal conductivity in both armchair and zigzag directions, which is qualitatively similar to the case of graphene.[51] For instance, the branch contributions to the total thermal conductivity are 67%, 13%, 10%, and 10% for ZA, TA, LA, and optical phonons along the zigzag direction. This is because the scattering rate for ZA phonon is the lowest in the entire Brillouin zone compared to other polarizations (Figs. 7(b)–7(d)). Besides, the scattering rate for ZA phonon in the armchair direction ($\Gamma \to X$) is slightly larger than that in the zigzag direction ($\Gamma \to Y$), as indicted by the dashed region in Fig. 7(b), which leads to a slightly lower thermal conductivity in armchair direction for ZA phonon. Similarly for LA phonon, the larger scattering rate in the armchair direction (Fig. 7(d)) results in a lower thermal conductivity in that direction. TA phonon, however, has the opposite trend, which has a larger scattering rate in the zigzag direction (Fig. 7(c)) and thus a lower thermal conductivity in that direction. The different chiral dependence for LA and TA phonons cancels with each other and thus reduces the anisotropy. Combined with the fact that negligible difference in ZA phonon's thermal conductivity between different directions, this leads to an almost isotropic thermal conductivity observed in Fig. 3(a), although its lattice structure is quite different in two directions.

In contrast, TA phonon makes the dominant contribution ($\sim 63\%$) to thermal conductivity of χ_3 borophene along the armchair direction (Fig. 8(a)). In the zigzag direction, although ZA phonon still has the largest contribution $\sim 38\%$, it only has a thermal conductivity ~ 118 W/(m·K), much lower than that of TA phonon ~ 330 W/(m·K) in the armchair direction. Therefore, the unusually dominant contribution from TA phonon along the armchair direction is responsible for the obvious anisotropic thermal conductivity observed in Fig. 3(b).

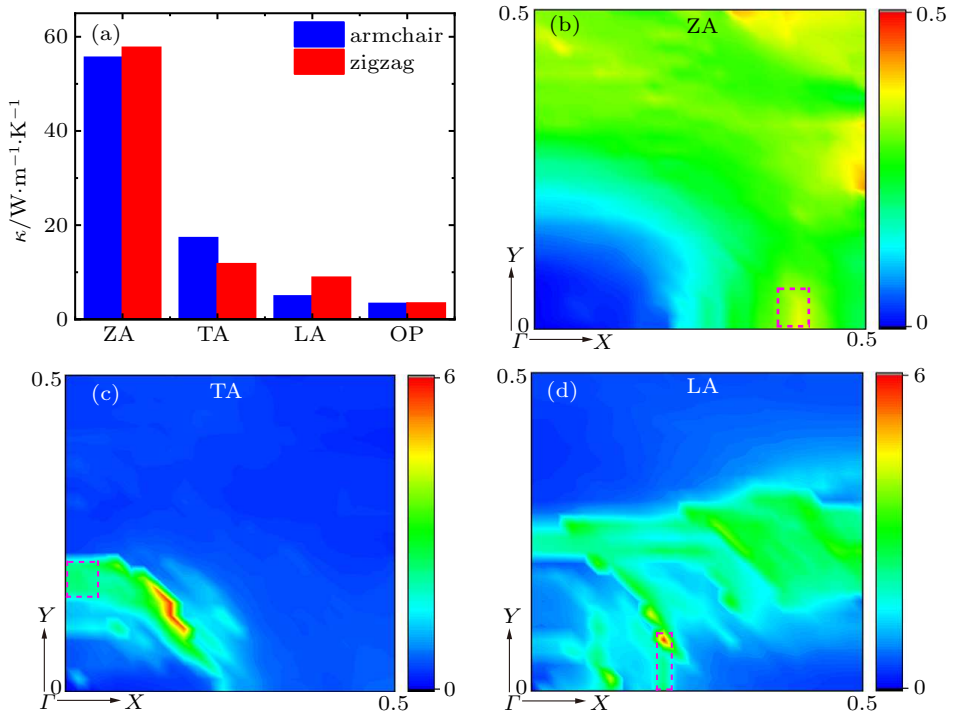


Fig. 7. (a) Branch contribution of thermal conductivity in β_{12} borophene at 300 K. Distribution of scattering rates (in units of cm^{-1}) in the Brillouin zone for (b) ZA, (c) TA, and (d) LA phonons. $\Gamma \to X$ represents the armchair direction, while $\Gamma \to Y$ represents the zigzag direction. The dashed box highlights the area of interest for comparison.

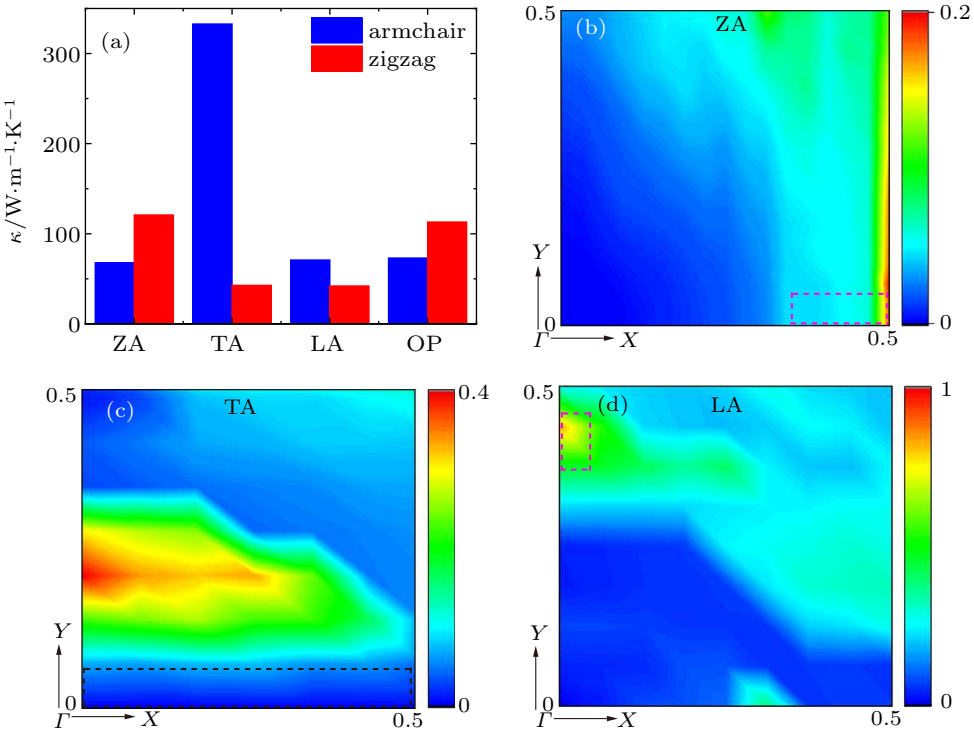


Fig. 8. (a) Branch contribution of thermal conductivity in χ_3 borophene at 300 K. Distribution of scattering rates (in units of cm^{-1}) in the Brillouin zone for (b) ZA, (c) TA, and (d) LA phonons. $\Gamma \rightarrow X$ represents the armchair direction, while $\Gamma \rightarrow Y$ represents the zigzag direction. The dashed box highlights the area of interest for comparison.

One remarkable feature in Fig. 8(a) is the huge contrast ratio of thermal conductivity in two directions for TA phonon around 900%, exhibiting a nearly one-dimensional thermal transport along armchair direction, while this ratio is only 150% and 159% for ZA and LA phonons, respectively. Therefore, anisotropic thermal transport is much weaker for ZA and LA phonons compared to TA phonon. This is because for both ZA and LA phonons, only a small portion of the Brillouin zone (dashed region in Figs. 8(b) and 8(d)) has a larger scattering rate in one direction compared to the other direction. Interestingly for TA phonon, there is a huge region with very strong scattering rate located in the middle of the Brillouin zone (Fig. 8(c)). This region with strong phonon scattering essentially blocks the TA phonon transport along the zigzag direction, and forces TA phonon to propagate along the armchair direction, in which negligible phonon scattering event is encountered (dashed region in Fig. 8(c)). In other words, the transport of TA phonon is almost one-dimensional along the armchair direction. We have further verified that the large relaxation time of TA phonons (dashed box in Fig. 5(b)) actually originates from those TA phonons in the dashed region in Fig. 8(c) which exhibit one-dimensional transport behavior.

Generally speaking, in planar structures such as graphene and β_{12} borophene, ZA phonons make the dominant contribution to heat transport.[51] And the traveling direction of phonons in a planar structure is usually random. Interestingly, the anomalous one-directional transport of TA phonon in χ_3 borophene leads to not only a very high thermal conductivity mainly contributed by TA phonon, but also a strong anisotropic thermal transport. A similar one-dimensional transport phenomenon occurs in the ballistic transport of δ_6 borophene and borophane.[47,48] This unique feature of χ_3 borophene may provide novel insights for enhancing the thermal conductivity of 2D materials.

Finally, we examine whether there exists hydrodynamic phonon transport in β_{12} and χ_3 borophene. Recent studies[74,75] have reported the unique hydrodynamic phonon transport behavior in two-dimensional materials, such as graphene, due to the significant role of momentum conserving normal process (N-process) of phonon–phonon scattering and dominant contribution of ZA phonon. In the relaxation time approximation for solving BTE, the N-process is incorrectly treated as the resistive process, similar to the Umklapp process (U-process). This leads to the underestimation of thermal conductivity compared to the iterative solution of BTE when the N-process is prevailing in the phonon–phonon scattering, which causes the hydrodynamic phonon transport. Therefore, the difference in thermal conductivity value between iterative solution and RTA solution can serve as an indication of hydrodynamic phonon transport.

As shown in Fig. 3, we find that there exists notable difference in thermal conductivity between the iterative solution (solid line) and RTA solution (dash-dot line) for both β_{12} and χ_3 borophene. For instance at 300 K, the iterative solution predicts thermal conductivity of 88 W/(m·K) and 94 W/(m·K) along the armchair and zigzag directions for β_{12} borophene,

while the RTA results are 52 W/(m·K) and 67 W/(m·K) along the armchair and zigzag directions, respectively. The ratio of $\kappa_{\text{iterative}}/\kappa_{\text{RTA}}$ in β_{12} borophene is around 1.7 and 1.4 along the armchair and zigzag directions, respectively, suggesting that hydrodynamic phonon transport takes place in β_{12} borophene. This is because of the prevailing normal process over the Umklapp process and the dominant contribution of ZA phonon in β_{12} borophene (Fig. 7(a)), similar to the case of graphene.[74,75] However, the ratio of $\kappa_{\text{iterative}}/\kappa_{\text{RTA}}$ at 300 K in χ_3 borophene is, respectively, only 1.1 and 1.2 along the armchair and zigzag directions, which is lower compared to the case of β_{12} borophene. This is because ZA phonon does not make the dominant contribution to thermal conductivity of χ_3 borophene (Fig. 8(a)), and thus the hydrodynamic effect is weaker compared to the case of β_{12} borophene.

4. Summary

Using first principle calculations combined with Boltzmann transport equation, we have systematically investigated the thermal transport in both β_{12} and χ_3 borophene. The room temperature thermal conductivity of β_{12} borophene is 88 W/(m·K) and 94 W/(m·K) along the armchair and zigzag directions, respectively, exhibiting almost isotropic thermal transport behavior. In contrast, the thermal conductivity of χ_3 borophene is much larger and highly anisotropic, reaching 512 W/(m·K) and 312 W/(m·K) at 300 K along the armchair and zigzag directions, respectively. This thermal conductivity value is almost comparable to that of h-BN, but is the highest among all known borophene allotropes. In β_{12} borophene, ZA phonon makes the dominant contribution to the thermal conductivity, and the contribution from ZA phonon is close to each other along the armchair and zigzag directions, leading to the isotropic thermal transport. More interestingly, the scattering rate distribution in the Brillouin zone reveals that TA phonon in χ_3 borophene transports almost one-directionally along the armchair direction with very weak scattering, which results in a substantially enhanced relaxation time for low-frequency TA phonon and consequently the anisotropic thermal transport in χ_3 borophene and the dominant contribution to thermal conductivity from TA phonon along the armchair direction. The high thermal conductivity of χ_3 borophene holds great promise in heat dissipation applications, which may provide a new way to realize large thermal conductivity in 2D systems.

References

[1] Pop E 2010 *Nano Res.* **3** 147
[2] Zhang Z and Chen J 2018 *Chin. Phys. B* **27** 35101
[3] Xu X, Zhou J and Chen J 2020 *Adv. Funct. Mater.* **30** 1904704
[4] Zhang Z, Hu S, Nakayama T, Chen J and Li B 2018 *Carbon* **139** 289
[5] Liu X, Zhang G and Zhang Y W 2015 *Carbon* **94** 760
[6] Yu Y, Wu L and Zhi J 2014 *Angew. Chem. Int. Ed.* **53** 14326
[7] Berber S, Kwon Y K and Tománek D 2000 *Phys. Rev. Lett.* **84** 4613
[8] Kim P, Shi L, Majumdar A and McEuen P L 2001 *Phys. Rev. Lett.* **87** 215502
[9] Balandin A A, Ghosh S, Bao W, Calizo I, Teweldebrhan D, Miao F and Lau C N 2008 *Nano Lett.* **8** 902
[10] Chen S, Wu Q, Mishra C, Kang J, Zhang H, Cho K, Cai W, Balandin A A and Ruoff R S 2012 *Nat. Mater.* **11** 203
[11] Seol J H, Jo I, Moore A L, Lindsay L, Aitken Z H, Pettes M T, Li X, Yao Z, Huang R, Broido D, Mingo N, Ruoff R S and Shi L 2010 *Science* **328** 213
[12] Chen J, Zhang G and Li B 2013 *Nanoscale* **5** 532
[13] Ghosh S, Bao W, Nika D L, Subrina S, Pokatilov E P, Lau C N and Balandin A A 2010 *Nat. Mater.* **9** 555
[14] Xu X, Pereira L F, Wang Y, Wu J, Zhang K, Zhao X, Bae S, Tinh Bui C, Xie R, Thong J T, Hong B H, Loh K P, Donadio D, Li B and Ozyilmaz B 2014 *Nat. Commun.* **5** 3689
[15] Castro Neto A H, Guinea F, Peres N M R, Novoselov K S and Geim A K 2009 *Rev. Mod. Phys.* **81** 109
[16] Wang J, Deng S, Liu Z and Liu Z 2015 *Nat. Sci. Rev.* **2** 22
[17] Zhang Z, Ouyang Y, Cheng Y, Chen J, Li N and Zhang G 2020 *Phys. Rep.* **860** 1
[18] Zhu X L, Liu P F, Zhang J, Zhang P, Zhou W X, Xie G and Wang B T 2019 *Nanoscale* **11** 19923
[19] Hu S, Zhang Z, Jiang P, Chen J, Volz S, Nomura M and Li B 2018 *J. Phys. Chem. Lett.* **9** 3959
[20] Xu X, Chen J and Li B 2016 *J. Phys.: Condens. Matter* **28** 483001
[21] Hu S, Zhang Z, Jiang P, Ren W, Yu C, Shiomi J and Chen J 2019 *Nanoscale* **11** 11839
[22] Xu W, Zhang G and Li B 2015 *J. Chem. Phys.* **143** 154703
[23] Gu X, Li B and Yang R 2016 *J. Appl. Phys.* **119** 085106
[24] Gu X, Wei Y, Yin X, Li B and Yang R 2018 *Rev. Mod. Phys.* **90** 041002
[25] Gu X, Fan Z, Bao H and Zhao C Y 2019 *Phys. Rev. B* **100** 064306
[26] Duan X, Wang C, Pan A, Yu R and Duan X 2015 *Chem. Soc. Rev.* **44** 8859
[27] Sorkin V, Cai Y, Ong Z, Zhang G and Zhang Y W 2016 *Crit. Rev. Solid. State Mater. Sci.* **42** 1
[28] Zhu L, Zhang G and Li B 2014 *Phys. Rev. B* **90** 214302
[29] Watanabe K, Taniguchi T and Kanda H 2004 *Nat. Mater.* **3** 404
[30] Zhang Z, Hu S, Chen J and Li B 2017 *Nanotechnology* **28** 225704
[31] Andrew J M, XiangFeng Z, Brian K, Joshua D W, Diego A, Benjamin D M, Xiaolong L, Brandon L F, Ulises S, Jeffrey R G, Miguel Jose Y, Arturo P, Artem R O, Mark C H and Nathan P G 2015 *Science* **350** 1513
[32] Feng B, Zhang J, Zhong Q, Li W, Li S, Li H, Cheng P, Meng S, Chen L and Wu K 2016 *Nat. Chem.* **8** 563
[33] Li D, Gao J, Cheng P, He J, Yin Y, Hu Y, Chen L, Cheng Y and Zhao J 2019 *Adv. Funct. Mater.* **30** 1904349
[34] Ranjan P, Sahu T K, Bhushan R, Yamijala S S, Late D J, Kumar P and Vinu A 2019 *Adv. Mater.* **31** 1900353
[35] Penev E S, Kutana A and Yakobson B I 2016 *Nano Lett.* **16** 2522
[36] Gao M, Li Q Z, Yan X W and Wang J 2017 *Phys. Rev. B* **95** 024505
[37] Yang J-Y, Zhang W, Xu C, Liu J, Liu L and Hu M 2020 *Int. J. Heat Mass Transf.* **152** 119481
[38] Li S, Wang A, Hu Y, Gu X, Tong Z and Bao H 2020 *Mater. Today Phys.* **15** 100256
[39] Zhou X F, Dong X, Oganov A R, Zhu Q, Tian Y and Wang H T 2014 *Phys. Rev. Lett.* **112** 085502
[40] Fan X, Ma D, Fu B, Liu C-C and Yao Y 2018 *Phys. Rev. B* **98** 195437
[41] Zhong C, Wu W, He J, Ding G, Liu Y, Li D, Yang S A and Zhang G 2019 *Nanoscale* **11** 2468
[42] Feng B, Sugino O, Liu R Y, Zhang J, Yukawa R, Kawamura M, Iimori T, Kim H, Hasegawa Y, Li H, Chen L, Wu K, Kumigashira H, Komori F, Chiang T C, Meng S and Matsuda I 2017 *Phys. Rev. Lett.* **118** 096401
[43] Feng B, Zhang J, Ito S, Arita M, Cheng C, Chen L, Wu K, Komori F, Sugino O, Miyamoto K, Okuda T, Meng S and Matsuda I 2018 *Adv. Mater.* **30** 1704025
[44] Wang L, Chen X, Du H, Yuan Y, Qu H and Zou M 2018 *Appl. Surf. Sci.* **427** 1030
[45] Rao D, Zhang L, Meng Z, Zhang X, Wang Y, Qiao G, Shen X, Xia H, Liu J and Lu R 2017 *J. Mater. Chem. A* **5** 2328
[46] Shukla V, Grigoriev A, Jena N K and Ahuja R 2018 *Phys. Chem. Chem. Phys.* **20** 22952
[47] Li D, He J, Ding G, Tang Q, Ying Y, He J, Zhong C, Liu Y, Feng C, Sun Q, Zhou H, Zhou P and Zhang G 2018 *Adv. Funct. Mater.* **28** 1801685

[48] Zhou H, Cai Y, Zhang G and Zhang Y W 2017 *npj 2D Mater. Appl.* **1** 14

[49] He J, Li D, Ying Y, Feng C, He J, Zhong C, Zhou H, Zhou P and Zhang G 2019 *npj Comput. Mater.* **5** 47

[50] Sun H, Li Q and Wan X G 2016 *Phys. Chem. Chem. Phys.* **18** 14927

[51] Lindsay L, Broido D A and Mingo N 2010 *Phys. Rev. B* **82** 115427

[52] Giannozzi P, Baroni S, Bonini N, Calandra M, Car R, Cavazzoni C, Ceresoli D, Chiarotti G L, Cococcioni M, Dabo I, Dal Corso A, de Gironcoli S, Fabris S, Fratesi G, Gebauer R, Gerstmann U, Gougoussis C, Kokalj A, Lazzeri M, Martin-Samos L, Marzari N, Mauri F, Mazzarello R, Paolini S, Pasquarello A, Paulatto L, Sbraccia C, Scandolo S, Sclauzero G, Seitsonen A P, Smogunov A, Umari P and Wentzcovitch R M 2009 *J. Phys.: Condens. Matter* **21** 395502

[53] Li W, Carrete J, A. Katcho N and Mingo N 2014 *Comput. Phys. Comm.* **185** 1747

[54] Fugallo G, Lazzeri M, Paulatto L and Mauri F 2013 *Phys. Rev. B* **88** 045430

[55] Batsanov S S 2001 *Inorg. Mater.* **37** 871

[56] Feng T, Lindsay L and Ruan X 2017 *Phys. Rev. B* **96** 161201

[57] Li S, Zheng Q, Lv Y, Liu X, Wang X, Huang P Y, Cahill D G and Lv B 2018 *Science* **361** 579

[58] Sang K J, Li M, Wu H, Nguyen H and Hu Y 2018 *Science* **361** 575

[59] Tian F, Song B, Chen X, Ravichandran N, Lv Y, Chen K, Sullivan S, Kim J, Zhou Y, Liu T-H, Goni M, Ding Z, Sun J, Gamage G A G U, Sun H, Ziyaee H, Huyan S, Deng L, Zhou J, Schmidt A J, Chen S, Chu C W, Huang P Y, Broido D, Shi L, Chen G and Ren Z 2018 *Science* **361** 582

[60] Gu X, Li S and Bao H 2020 *Int. J. Heat Mass Transf.* **160** 120165

[61] Zhang Z, Chen J and Li B 2017 *Nanoscale* **9** 14208

[62] Broido D A, Ward A and Mingo N 2005 *Phys. Rev. B* **72** 014308

[63] Wang Z, Lu T Y, Wang H Q, Feng Y P and Zheng J C 2016 *Phys. Chem. Chem. Phys.* **18** 31424

[64] Carrete J, Li W, Lindsay L, Broido D A, Gallego L J and Mingo N 2016 *Mater. Res. Lett.* **4** 204

[65] Zhang Z, Yang Y, Penev E S and Yakobson B I 2017 *Adv. Funct. Mater.* **27** 1605059

[66] Lindsay L, Li W, Carrete J, Mingo N, Broido D A and Reinecke T L 2014 *Phys. Rev. B* **89** 155426

[67] Lindsay L and Broido D A 2012 *Phys. Rev. B* **85** 035438

[68] Mortazavi B, Makaremi M, Shahrokhi M, Raeisi M, Singh C V, Rabczuk T and Pereira L F C 2018 *Nanoscale* **10** 3759

[69] Liu G, Wang H, Gao Y, Zhou J and Wang H 2017 *Phys. Chem. Chem. Phys.* **19** 2843

[70] Peng B, Zhang H, Shao H, Xu Y, Zhang X and Zhu H 2016 *Ann. Phys.* **528** 504

[71] Qin G, Yan Q B, Qin Z, Yue S Y, Hu M and Su G 2015 *Phys. Chem. Chem. Phys.* **17** 4854

[72] Peng B, Zhang H, Shao H, Xu Y, Zhang X and Zhu H 2016 *Sci. Rep.* **6** 20225

[73] Becke A D and Edgecombe K E 1990 *J. Chem. Phys.* **92** 5397

[74] Cepellotti A, Fugallo G, Paulatto L, Lazzeri M, Mauri F and Marzari N 2015 *Nat. Commun.* **6** 6400

[75] Lee S, Broido D, Esfarjani K and Chen G 2015 *Nat. Commun.* **6** 6290